CHINESE OPTICS LETTERS

Vol. 19, No. 10 | October 2021

Narrow vertical beam divergence angle for display applications of 645 nm lasers

Yufei Jia (贾宇飞)[1,2], Yufei Wang (王宇飞)[1,3], Xuyan Zhou (周旭彦)[1], Linhai Xu (徐林海)[1,2], Pijie Ma (马丕杰)[1,3], Jingxuan Chen (陈静瑄)[1,2], Hongwei Qu (渠红伟)[1], and Wanhua Zheng (郑婉华)[1,2,3,4*]

[1] Laboratory of Solid State Optoelectronics Information Technology, Institute of Semiconductors, Chinese Academy of Sciences, Beijing 100083, China

[2] Center of Materials Science and Optoelectronics Engineering, University of Chinese Academy of Sciences, Beijing 100049, China

[3] College of Future Technology, University of Chinese Academy of Sciences, Beijing 101408, China

[4] State Key Laboratory on Integrated Optoelectronics, Institute of Semiconductors, Chinese Academy of Sciences, Beijing 100083, China

*Corresponding author: whzheng@semi.ac.cn

Received January 21, 2021 | Accepted March 9, 2021 | Posted Online August 5, 2021

We design a 645 nm laser diode (LD) with a narrow vertical beam divergence angle based on the mode expansion layer. The vertical beam divergence of 10.94° at full width at half-maximum is realized under 1.5 A continuous-wave operation, which is the smallest vertical beam divergence for such an LD based on the mode expansion layer, to the best of our knowledge. The threshold current and output power are 1.07 A and 0.94 W, limited by the thermal rollover for the 100 μm wide and 1500 μm long broad area laser, and the slope efficiency is 0.71 W/A. The low coherence device is fabricated with the speckle contrast of 3.6% and good directional emission. Such 645 nm LDs have promising applications in laser display.

Keywords: beam divergence; laser diode; speckle; laser display.
DOI: 10.3788/COL202119.101401

1. Introduction

Applications of laser diodes (LDs) have been widely spreading into many areas, from the industrial manufacturing like welding and cutting to daily life such as data storage and telecommunication. Red-emitting laser sources play an important role in the medical field and digital appliances[1–3]. As the laser-based display develops rapidly, red LDs have attracted much more attention[4–8]. Red LDs have natural merits such as wider color gamut, more compact size, and so on, compared with the traditional light sources such as lamps and light-emitting diodes (LEDs). However, some drawbacks exist in the practical application of red LDs. Red LDs are based on AlGaInP/InGaP material, which has a lower thermal conductivity and smaller conduction band offset (ΔE_c) compared with AlGaAs/GaAs. The traditional red LDs have large vertical far-field divergence of about 40°. This leads to a poor coupling efficiency and a small alignment tolerance between the laser and other optical elements[9]. Moreover, the coherent artifacts like speckles degrade the imaging quality owing to the inherent nature of lasers. To solve the first problem, AlGaAs working as the material of the p-side cladding has been demonstrated by Unger *et al.*[10]. Many approaches, such as thin active layer, leaky-wave and tilted-wave layer, large optical cavity (LOC), photonic band crystal (PBC) lasers, and the mode expansion layers structure, were adopted to narrow down the vertical beam divergence angle[11–17]. A vertical divergence of 12.7° at the full width at half-maximum (FWHM) has been reported based on the mode expansion layer[18]. For the second problem, the low coherence electrically pumped semiconductor lasers have been presented, aiming at reducing the speckle contrast from the source[19–22].

In this Letter, we adopt the structure of the mode expansion layer to narrow down the vertical beam divergence and analyze the mode behavior in the vertical direction. A low vertical divergence angle of 10.94° is realized in the experiment. The peak power of the broad area (BA) laser can reach 0.94 W, limited by the thermal rollover under continuous-wave (CW) operation. Furthermore, we fabricate the low coherence red LD device, which can achieve speckle contrast of 3.6% and peak power of 1.42 W under pulsed operation. This red LD can also realize the directional emission in both lateral and vertical directions.

2. Passive Mode Analysis and Structure Design

The refractive index of AlGaInP is critical to the calculation of the near-field amplitude, which further influences the far-field intensity profile. We adopt the modified single effective oscillator (MSEO) and related parameters to ensure the accuracy of refractive index of the layers[23,24]. Accordingly, we show the sectional refractive index profile and the near-field pattern

(NFP) of the designed structure in Fig. 1. The calculated optical confinement factor (Γ) is 3.133%.

In the epitaxial direction, the following layers include 0.1 μm GaInP:Si *n*-buffer layer, 2.5 μm *n*-cladding layer $(Al_{0.68}Ga_{0.32})In_{0.49}P$:Si, 1.2 μm mode expansion layer $(Al_{0.7}Ga_{0.3})In_{0.49}P$:Si, and the 1 μm p-cladding layer $Al_{0.51}In_{0.49}P$:Mg, followed the 0.05 μm highly p-doped buffer layer GaInP:Mg and 0.2 μm GaAs:C cap layer. The active region consists of 0.05 μm undoped $(Al_{0.5}Ga_{0.5})In_{0.49}P$ waveguide layers and compressively strained GaInP triple quantum wells (QWs) with a thickness of 5 nm, where the wells are separated by 10 nm $(Al_{0.5}Ga_{0.5})In_{0.49}P$ barrier layers.

The maximum conduction band offset (ΔE_c) of the AlGaInP material system is about 270 meV, while that of the AlGaAs is 350 meV[25], which leads to carrier leakage from the active region to the cladding layer, especially at a shorter wavelength. As shown in Fig. 2, we calculate the conduction energy band at the different p-cladding layer doping levels. According to the inset, the ΔE_c increases when the doping concentration of the p-cladding layer increases under a high p-doping level. Considering the practical growth conditions, we choose the doping level of 6×10^{17}cm^{-3} for the p-cladding layer with Mg, in which ΔE_c is 227 meV. Furthermore, we design an asymmetric structure, and $Al_{0.51}In_{0.49}P$ is used as the p-cladding layer with a low refractive index, which can expand the near field into the *n* side to avoid the large free-carrier absorption in the p-cladding layer.

The thicknesses of the cladding layer ($d_{n-\text{cladding}}$) and mode expansion layer (d_{ME}) have critical influences on the near field and vertical divergence. We theoretically calculate the vertical divergence angle, which is based on the parameters mentioned above. At the first step, the mode characteristics with a constant $d_{n-\text{cladding}}$ of 1.8 μm and different d_{ME} are studied. Figure 3(a) shows the dependence of the calculated Γ, vertical divergence angle at FWHM, and $R_{\text{F/H}}$ on the d_{ME}, where the $R_{\text{F/H}}$ is defined as the ratio between Γ of the fundamental mode and the largest

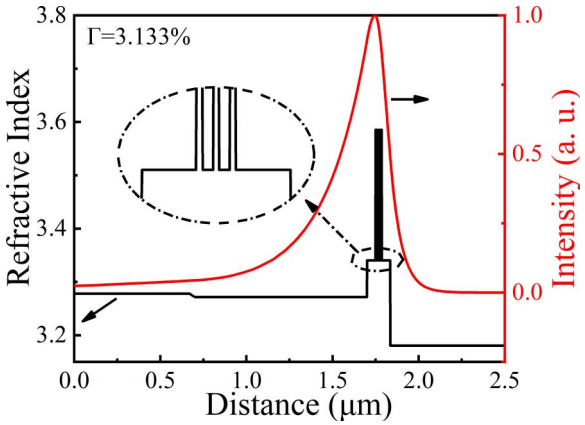

Fig. 1. Schematic of the sectional refractive index distribution (left axis) and the optical NFP distribution (right axis). The inset shows the detail of the active region.

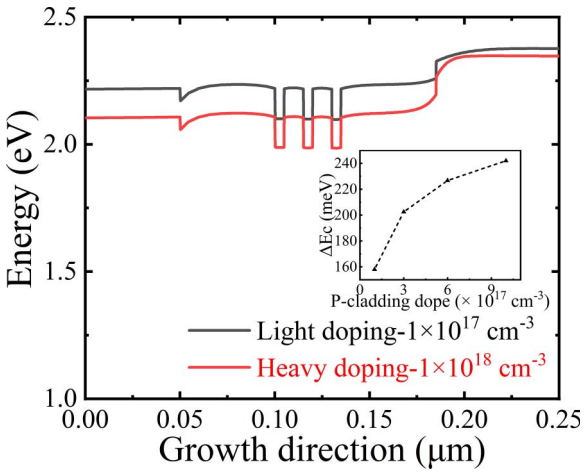

Fig. 2. Calculated conduction energy band diagram at different doping levels. The inset shows the ΔE_c between the waveguide layer and the p-cladding layer at different doping levels.

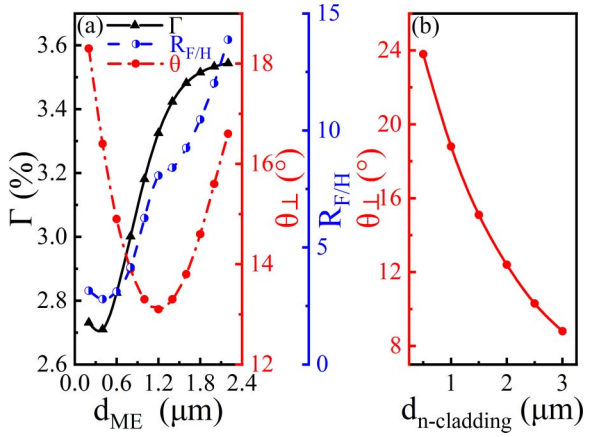

Fig. 3. (a) Dependence of calculated Γ, vertical divergence, and $R_{\text{F/H}}$ on d_{ME}; (b) dependence of vertical divergence on $d_{n-\text{cladding}}$.

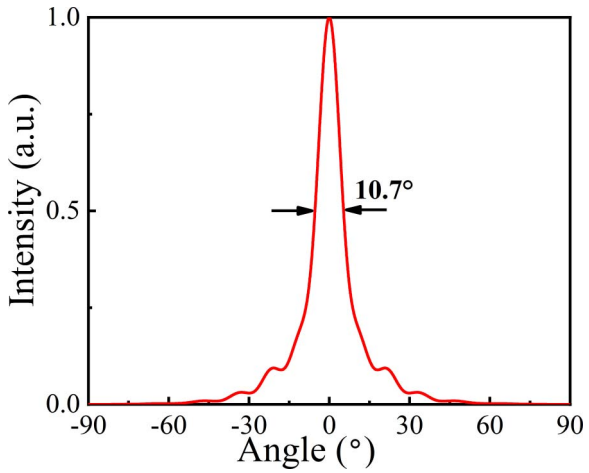

Fig. 4. Simulated far-field pattern (FFP) in the fast axis.

confinement factor among the high-order modes. Γ and $R_{F/H}$ increase as d_{ME} is increased, and the lowest vertical divergence is realized at a medium thickness of 1.2 μm. Second, the far-field characteristic with a constant d_{ME} of 1.2 μm is studied. Figure 3(b) depicts the vertical divergence decreasing with the increased $d_{n-cladding}$. For the low vertical divergence structure, the $d_{n-cladding}$ is set to 2.5 μm. Based on the analysis above, the d_{ME} of 1.2 μm and the $d_{n-cladding}$ of 2.5 μm are chosen for the structure. Figure 4 shows the calculated vertical divergence angle, and a vertical divergence angle of 10.7° is obtained.

In order to realize the low coherence, we prefer to have a number of modes lasing simultaneously by designing the cavity structure. We directly fabricate the low coherence LD according to the good results in our previous work[21,22].

3. Device Fabrication and Results

The epitaxial layer is grown by metal organic chemical vapor deposition (MOCVD) on a Si-doped misoriented GaAs substrate tilted 15° off (100) toward [111]. The BA lasers are formed by photolithography and dry etching, and SiO_2 film is deposited as the electrical isolation layer. The injected window is opened by the wet chemical etching. Ti/Pt/Au is sputtered on the top of the highly doped p-GaAs layer, which used the PVD method for ohmic contact. The GaAs substrate is thinned down to the 130 μm via mechanical polishing. Finally, the AuGeNi/Au is grown on the *n* side by PVD and annealed at 420°C.

Uncoated BA lasers are fabricated to obtain parameters such as the internal quantum efficiency (η_i), internal optical loss (α_i), modal gain (ΓG_0), and transparent current density (J_{tr}), which can quantitatively assess the quality of the wafer. The BA lasers have a width of 100 μm and different lengths varying from 0.5 mm to 3 mm. The lasers are measured in the pulsed mode with a pulse width of 40 μs at a repetition rate of 100 Hz at 20°C. Figure 5(a) shows the typical cavity length dependence of the inverse external differential quantum efficiency ($1/\eta_d - L$). We can fit the experimental results and obtain η_i of 71% and α_i of 3.95 cm^{-1}. Figure 5(b) is the representation of threshold current density J_{th} versus the inverse cavity length $1/L$ for lasers of different cavity lengths. J_{tr} of 444.08 A/cm^2 and ΓG_0 of 37.98 cm^{-1} are extracted from the fitting curve.

We adopt Al_2O_3 as a facet mirror passivation coating. The front facet is coated with 10% anti-reflection (AR) layer, and the rear facet is coated with a 99% reflectivity layer for high reflection (HR). Figure 6 shows the light–current–voltage (*L*–*I*–*V*) and wall plug efficiency (WPE) curves for the device with a cavity length of 1500 μm and a width of 100 μm under 3 A CW at 20°C. The LD has a slope efficiency of 0.71 W/A, a threshold of 1.07 A, and the maximum WPE of 16.04% at 2.3 A. The maximum power of 0.94 W is achieved at 2.7 A, limited by the thermal rollover. The inset shows the emitting peak wavelength at 647.54 nm with an FWHM of 0.65 nm at 1.5 A CW.

The contrast of the vertical far-field profile is presented in Fig. 7. We obtain the vertical far-field divergence as low as

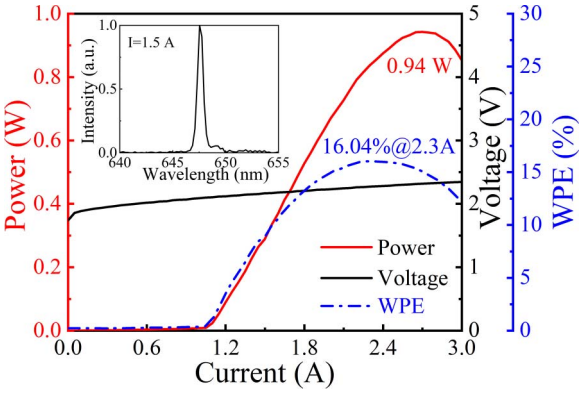

Fig. 6. Experimental *L*–*I*–*V* and WPE characteristics for 100 μm BA laser with a 1500 μm long cavity. The laser device is operated with coated AR of 10% and HR of 99% under 3 A CW at 20°C heatsink temperature. The inset shows the spectrum at 1.5 A CW.

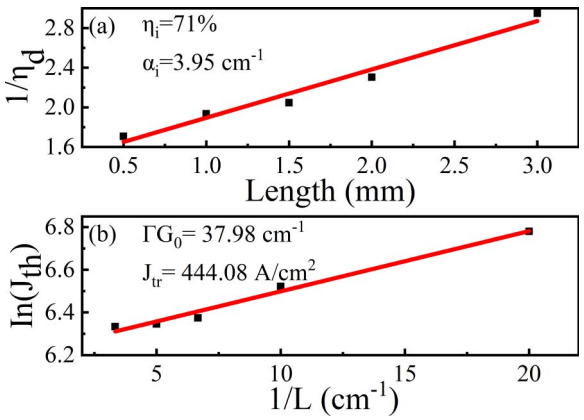

Fig. 5. (a) Cavity length dependence of the inverse external differential quantum efficiency; (b) threshold current density versus the inverse cavity length.

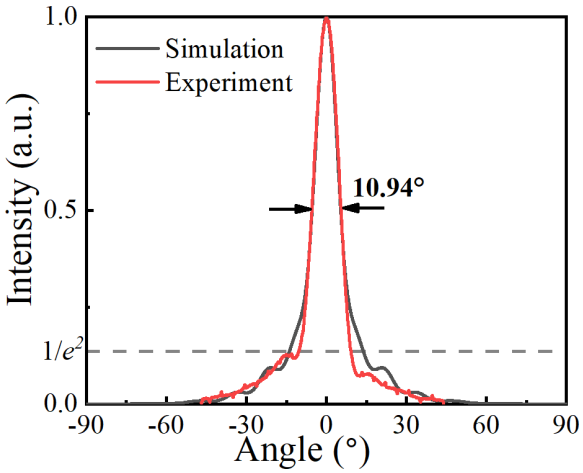

Fig. 7. FFP of simulation and experiment. The dashed line indicates $1/e^2$ of the peak value.

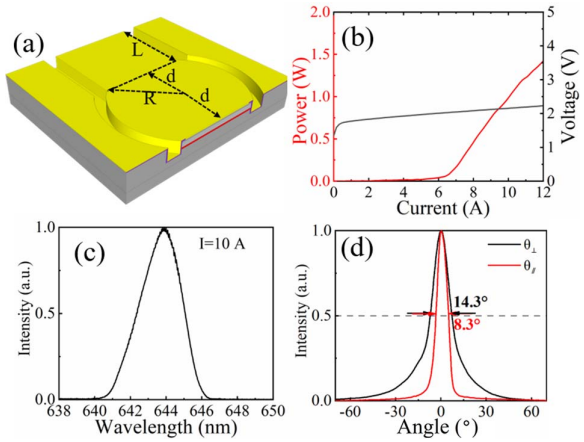

Fig. 8. (a) Schematic of the low coherence red LD structure; (b) *L*–*I*–*V* curves; (c) the spectrum at 10 A; (d) the FFP at 10 A.

10.94° (FWHM) and 19.7° ($1/e^2$) measured at 1.5 A CW at 20°C, which agrees well with the theoretical result.

To the best of our knowledge, the vertical divergence of 10.94° is the smallest for the red LD based on the mode expansion layer, other than the longitudinal photonic crystal structure.

Figure 8(a) shows the schematic of the low coherence red LD structure. The sizes of the *R*, *d*, and *L* are 500 μm, 250 μm, and 1000 μm, respectively. Lasers are tested in pulsed mode with a 40 μs width and 100 Hz repetition rate. The corresponding *L*–*I*–*V* curves are measured under the same condition at 20°C. The peak power of 1.42 W is obtained at 12 A, as shown in Fig. 8(b). Figure 8(c) shows the spectrum at 10 A at 20°C. The peak wavelength is 643.7 nm with the FWHM of 2.73 nm. Figure 8(d) exhibits the far-field pattern (FFP) with 8.3° × 14.3° (FWHM) at the current of 10 A, which shows a better directional emission[20].

The vertical divergence angles between the low coherence LD and BA LD are different. We doubt that the possible reasons are the lateral mode oscillation and the different test conditions due to the test equipment.

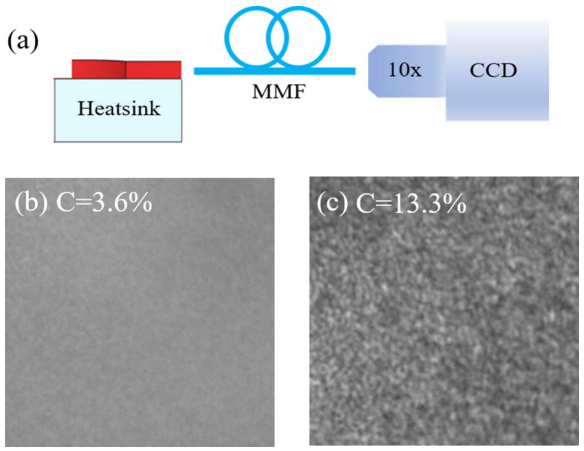

Fig. 9. (a) Schematic of the experimental setup of the speckle measurement; (b) speckle pattern of low coherence red LD structure; (c) speckle pattern of BA laser.

We characterize the low coherence by the speckle contrast. Figure 9(a) shows the schematic of the experimental setup of the speckle measurement. The light emitted from laser is coupled into a fiber (core diameter = 1 mm, NA = 0.5, length = 1 m) and collected by the CCD camera (Lt545R, Lumenera) with the pixel size of 3.45 μm × 3.45 μm. We adopt the 300 × 300 pixels to calculate the speckle contrast. Figure 9(b) shows the speckle pattern of the low coherence red LD structure, and the speckle contrast is reduced to 3.6%, compared with the 13.3% of the BA laser. We can estimate that the approximate 771 modes lase independently[20].

4. Conclusion

We have demonstrated red LDs with a narrow vertical far field in the 645 nm range. An efficient mode expansion layer is designed to produce a strong penetration of the near-field distribution, which is beneficial to narrow down the FFP. A narrow vertical far-field angle of 10.94° is achieved experimentally. The maximum output power of 0.94 W at 2.7 A, limited by the thermal rollover, is achieved under the CW condition.

We have realized red LDs with a low coherence and directional emission with this epitaxy structure. The peak power of 1.42 W and the lateral divergence of 8.3° are achieved under pulsed operation. The speckle contrast is reduced to 3.6%, which means it has a bright prospect in laser display. With the optimization of epitaxial layers, the low coherence red LD can operate at the CW condition.

Acknowledgement

This work was supported in part by the National Key R&D Program of China (Nos. 2016YFB0401804 and 2016YFA0301102) and the National Natural Science Foundation of China (Nos. 91850206 and 62075213).

References

1. M. M. He, S. Chen, Q. X. Na, S. J. Luo, H. Y. Zhu, Y. Li, C. W. Xu, and D. Y. Fan, "Watt-level Pr^{3+}:YLF deep red laser pumped by a fiber-coupled blue LD module or a single-emitter blue LD," Chin. Opt. Lett. **18**, 011405 (2020).
2. T. Yagi, H. Nishiguchi, Y. Yoshida, M. Miyashita, M. Sasaki, Y. Sakamoto, K. Ono, and Y. Mitsui, "High-power high-efficiency 660-nm laser diodes for DVD-R/RW," IEEE J. Sel. Top. Quantum Electron. **9**, 1260 (2003).
3. C. Y. Chen, H. T. Chang, T. J. Chang, and C. H. Chuang, "Full-color and less-speckled modified Gerchberg–Saxton algorithm computer-generated hologram floating in a dual-parabolic projection system," Chin. Opt. Lett. **13**, 110901 (2015).
4. H. Kawanishi, "IR/R/G/B laser diodes for multi-wavelength applications," Opt. Rev. **26**, 152 (2019).
5. Z. Y. Xu, "Laser displays—new display technology for next generation," Laser Infrared **36**, 737 (2006).
6. T. Nishida, K. Kuramoto, Y. Iwai, T. Fujita, and T. Yagi, "Multiemitter 638-nm high-power broad area laser diodes for display application," Opt. Eng. **58**, 086113 (2019).

7. M. Hagimoto, S. Miyamoto, Y. Kimura, H. Fukai, M. Hashizume, and S. Kawanaka, "USHIO 3.5W red laser diode for projector light source," Proc. SPIE **10939**, 109391I (2019).
8. K. Paschkel, G. Blume, D. Feise, J. Pohl, and B. Sumpf, "Watt-level red-emitting diode lasers and modules for display applications," Opt. Rev. **23**, 146 (2016).
9. B. Sverdlov, H.-U. Pfeiffer, E. Zibik, S. Mohrdiek, T. Pliska, M. Agresti, and N. Lichtenstein, "Optimization of fiber coupling in ultra-high power pump modules at λ = 980 nm," Proc. SPIE **8605**, 860508 (2013).
10. P. Unger, G.-L. Bona, R. Germann, P. Roentgen, and D. J. Webb, "Low-threshold strained GaInP quantum-well ridge lasers with AlGaAs cladding layers," IEEE J. Quantum Electron. **29**, 1880 (1993).
11. K. Hamada, M. Wada, H. Shimizu, M. Kume, F. Susa, T. Shibutani, N. Yoshikawa, K. Itoh, G. Kano, and I. Teramoto, "A 0.2 W CW laser with buried twin-ridge substrate structure," IEEE J. Quantum Electron. **21**, 623 (1985).
12. N. B. Zvonkov, B. N. Zvonkov, A. V. Ershov, E. A. Uskova, and G. A. Maksimov, "Semiconductor lasers emitting at the 0.98 μm wavelength with radiation coupling-out through the substrate," Quantum Electron. **28**, 605 (1998).
13. V. Shchukin, N. Ledentsov, K. Posilovic, V. Kalosha, T. Kettler, D. Seidlitz, M. Winterfeldt, D. Bimberg, N. Y. Gordeev, L. Y. Karachinsky, I. I. Novikov, Y. M. Shernyakov, A. V. Chunareva, M. V. Maximov, F. Bugge, and M. Weyers, "Tilted wave lasers: a way to high brightness sources of light," IEEE J. Quantum Electron. **47**, 1014 (2011).
14. S. Zhao, A. Qi, M. Wang, H. Qu, Y. Lin, F. Dong, and W. Zheng, "High-power high-brightness 980 nm lasers with >50% wall-plug efficiency based on asymmetric super large optical cavity," Opt. Express **26**, 3518 (2018).
15. L. Liu, H. Qu, Y. Liu, Y. Wang, A. Qi, X. Guo, P. Zhao, Y. Zhang, and W. Zheng, "Design and analysis of laser diodes based on the longitudinal photonic band crystal concept for high power and narrow vertical divergence," IEEE J. Sel. Top. Quantum Electron. **21**, 1900107 (2015).
16. P. M. Smowton, G. M. Lewis, M. Yin, H. D. Summers, G. Berry, and C. C. Button, "650-nm lasers with narrow far-field divergence with integrated optical mode expansion layers," IEEE J. Sel. Top. Quantum Electron. **5**, 735 (1999).
17. B. Qiu, O. P. Kowalski, S. McDougall, B. Schmidt, and J. H. Marsh, "High-performance red lasers with low beam divergence," IEEE Photon. J. **1**, 172 (2009).
18. P. M. Smowton and S. N. Elliott, "Manufacturing-tolerant compact red-emitting laser diode designs for next generation applications," IET Optoelectron. **9**, 75 (2015).
19. B. Redding, A. Cerjan, X. Huang, M. L. Lee, A. D. Stone, M. A. Choma, and H. Cao, "Low spatial coherence electrically pumped semiconductor laser for speckle-free full-field imaging," Proc. Natl. Acad. Sci. USA **112**, 1304 (2015).
20. K. Kim, S. Bittner, Y. Zeng, SF. Liew, Q. Wang, and H. Cao, "Electrically pumped semiconductor laser with low spatial coherence and directional emission," Appl. Phys. Lett. **115**, 071101 (2019).
21. Y. Jia, Y. Wang, L. Xu, S. Zhao, A. Qi, and W. Zheng, "Low-spatial coherence electrically pumped red-emitting semiconductor laser," Proc. SPIE **10812**, 108120V (2018).
22. L. Xu, Y. Wang, Y. Jia, and W. Zheng, "Low-coherence, high-power, high-directional electrically driven dumbbell-shaped cavity semiconductor laser at 635 nm," Opt. Lett. **45**, 5097 (2020).
23. M. A. Afromowitz, "Refractive index of $Ga_{1-x}Al_xAs$," Solid State Commun. **15**, 59 (1974).
24. G. Hatakoshi, K. Itaya, M. Ishikawa, M. Okajima, and Y. Uematsu, "Short-wavelength InGaAlP visible laser diodes," IEEE J. Quantum Electron. **27**, 1476 (1991).
25. D. P. Bour, "Strained $Ga_xIn_{1-x}P$-$(AlGa)_{0.5}In_{0.5}P$ heterostructures and quantum-well laser diodes," IEEE J. Quantum Electron. **30**, 593 (1994).